Redox Potential of Quinones in Photosynthetic Reaction Centers from *Rhodobacter sphaeroides*: Dependence on Protonation of Glu-L212 and Asp-L213[†]

Hiroshi Ishikita, Giulia Morra, and Ernst-Walter Knapp*

Institute of Chemistry, Department of Biology, Chemistry, and Pharmacy, Free University of Berlin, Takustrasse 6, D-14195 Berlin, Germany

Received September 3, 2002; Revised Manuscript Received January 29, 2003

ABSTRACT: The absolute values of the one-electron redox potentials of the two quinones (Q_A and Q_B) in bacterial photosynthetic reaction centers from *Rhodobacter sphaeroides* were calculated by evaluating the electrostatic energies from the solution of the linearized Poisson−Boltzmann equation at pH 7.0. The redox potential for Q_A was calculated to be between −173 and −160 mV, which is close to the lowest measured values that are assumed to refer to nonequilibrated protonation patterns in the redox state Q_A^-. The redox potential of quinone Q_B is found to be about 160−220 mV larger for the light-exposed than for the dark-adapted structure. These values of the redox potentials are obtained if Asp-L213 is nearly protonated (probability 0.75−1.0) before and after electron transfer from Q_A to Q_B, while Glu-L212 is partially protonated (probability 0.6) in the initial state $Q_A^-Q_B^0$ and fully protonated in the final state $Q_A^0Q_B^-$. Conversely, if the charge state of the quinones is varied from $Q_A^-Q_B^0$ to $Q_A^0Q_B^-$ corresponding to the electron transfer from Q_A to Q_B, Asp-L213 remains protonated, while Glu-L212 changes its protonation state from 0.15 H^+ to fully protonated. In agreement with results from FTIR spectra, there is proton uptake at Glu-L212 going along with the electron transfer, whereas Asp-L213 does not change its protonation state. However, in our simulations Asp-L213 is considered to be protonated rather than ionized as deduced from FTIR spectra. The calculated redox potential of Q_A shows little dependence on the charge state of Asp-L213, which is due to a strong coupling with the protonation state of Asp-M17 but increases by 50 mV if Glu-L212 changes from the ionized to the protonated charge state. Both are in agreement with fluorescence measurements observing the decay of $SP^+Q_A^-$ in a wide pH regime. The computed difference in redox potential of Q_B in the light-exposed and dark-adapted structure was traced back to the hydrogen bond of Q_B with His-L190 that is lost in the dark-adapted structure and the charge of the non-heme iron atom, which is closer to Q_B in the light-exposed than in the dark-adapted structure.

The bacterial photosynthetic reaction center (RC)[1] from *Rhodobacter sphaeroides* consists of three subunits, the L, M, and H chain, and four bacteriochlorophyll *a*, two bacteriopheophytin *a*, and two ubiquinones as cofactors. These cofactors embedded in subunit L and M are arranged in two branches (A and B) that are related by a C_2 symmetry with an axis going through the center of the special pair (SP) (a strongly interacting dimer of bacteriochlorophyll *a*) and the non-heme iron atom. In general, only the A-branch is electron-transfer active, although recently with blue light excitation electron transfer along the B-branch for an RC with both quinones removed was observed, too (*1*). In a complex sequence of events, the RC converts light energy into electrostatic energy that is stored as proton gradient. The electronic excitations of the light harvesting chromophors are transferred to the SP where the charge separation process occurs. Thereby, an electron is transferred on a picosecond time scale to the bacteriopheophytin a of the A-branch and from there on a subnanosecond time scale to the ubiquinone of the A-branch (Q_A) and finally on the microsecond time scale to the ubiquinone of the B-branch (Q_B). After this first electron-transfer process, a second electron is transferred from Q_A to Q_B, and Q_B takes up two protons forming a dihydroquinone Q_BH_2, which leaves the binding pocket.

Before the first electron can be transferred from Q_A to Q_B, a conformational change (*2*−*6*) in the RC structure must occur. One of the first hints for this mechanism came from the finding that the electron transfer from Q_A to Q_B did not occur on samples of RCs from *R. sphaeroides*, which were frozen in the dark (*5*). The structural differences were elucidated from the dark-adapted and light-exposed crystal structures (*7*). On the basis of these observations, the idea of conformational gating of the electron transfer from $Q_A^-Q_B$ to $Q_AQ_B^-$ was put forward experimentally (*8*) and theoretically (*9*, *10*). The two crystal structures differ mainly in the

[†] This work was supported by the Deutsche Forschungsgemeinschaft SFB 498, Project A5, GRK 80/2, GRK 268, GKR 788/1, and the Fond der Chemischen Industrie with the BMFT. H.I. was supported by the DAAD.

* Corresponding author. Fax: (+49)30-83853464. E-mail: knapp@chemie.fu-berlin.de.

[1] Abbreviations: AA mutant, double mutant E(L212)A and D(L213)A; CHARMM, Chemistry at Harvard Molecular Mechanics; FTIR, Fourier transform infrared; LH1, light harvesting complex 1; LPBE, linearized Poisson−Boltzmann equation; MC, Monte Carlo; MD, molecular dynamics; PDB, protein data bank; Q_A, ubiquinone in the active A-branch of the RC; Q_B, ubiquinone in the inactive B-branch of the RC; *R. sphaeroides*, *Rhodobacter sphaeroides*; *R. capsulatus*, *Rhodobacter capsulatus*; RC, reaction center; SP, special pair.

10.1021/bi026781t CCC: $25.00 © 2003 American Chemical Society
Published on Web 03/12/2003

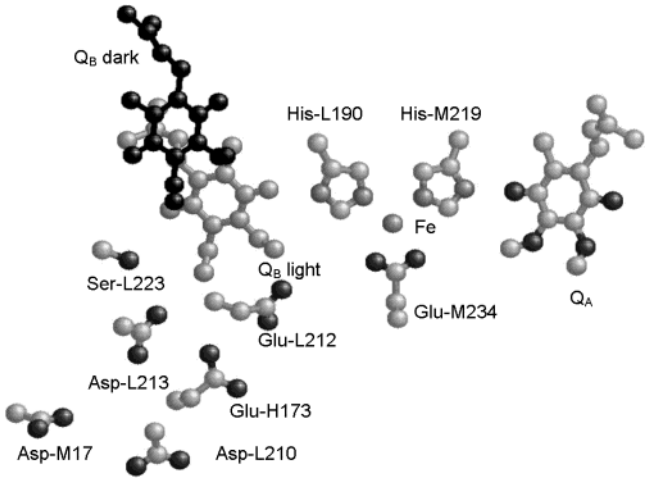

FIGURE 1: Side chains of residues relevant for the electron transfer between the quinones and the coupled proton transfer in RC from *R. sphaeroides*. In the light-exposed structure, Q_B is at a position proximal to the non-heme iron. In the dark-adapted structure, it is at the distal position. In this work we focus on Glu-L212 and Asp-L213.

conformation of Q_B. In the dark-adapted structure, where the electron cannot be transferred from Q_A to Q_B, Q_B is displaced by about 5 Å relative to the light-exposed structure and has undergone a propeller twist by 180° (Figure 1). The gating mechanism requires that the electron recedes at Q_A until Q_B undergoes a conformational change from the dark-adapted to the light-exposed structure. It is an open question whether the reduced Q_A induces the conformational change at Q_B or whether the conformational change at Q_B occurs spontaneously by thermal fluctuation and is stabilized after reducing the Q_B. In the light-exposed structure, a network of hydrogen bonds involving two chains of water molecules exists in the vicinity of Q_B connecting the protein surface with Q_B and providing a channel for the proton uptake by Q_B (*7*, *11*).

The interactions of the residues Glu-L212 and Asp-L213 (Figure 1) with Q_B are crucial for the first electron transfer from Q_A to Q_B, which is followed by a proton uptake process at Q_B. Except for Ser-L223 whose OH group is protonated and generally not titratable, the protonation states of the acidic residues in the neighborhood of Q_B are known to have a strong influence on the energetics of the electron-transfer process between the two quinones. Several experimental approaches have been used to estimate the protonation state of the acidic residues in the vicinity of Q_B by kinetic studies on point-mutated RCs (*12*, *13*) and by recording FTIR spectra (*14*, *15*). However, the interpretation of experiments probing the protonation state of the key residues Glu-L212 and Asp-L213 for the different redox states $Q_A^-Q_B$ and $Q_AQ_B^-$ remains ambiguous, despite vigorous quests to identify the titration behavior of the individual residues.

To reveal the mutual dependence of the protonation states of the key residues Glu-L212 and Asp-L213 on the redox states of the quinones, it is crucial to understand details of the electron-transfer reaction mechanism. For instance, it was pointed out that previous analyses of the time dependence of electron-transfer data may be oversimplified (*16*). Furthermore, there are still discrepancies regarding the protonation state that depend on the method of analysis. From molecular dynamics (MD) simulation (*17*), it was concluded that Asp-L213 is protonated in the $Q_AQ_B^-$ state, whereas experiments on kinetic data (*18*−*20*) and FTIR spectra (*14*, *16*) implied an ionized Asp-L213.

The majority of experimental and theoretical work focuses on the difference of the redox potentials between Q_A and Q_B that is driving the electron-transfer reaction. In this work, we are computing the values of the absolute in situ redox potentials of both quinones in the RC from *R. sphaeroides* separately as a function of the charge states of the acidic residues Glu-L212 and Asp-L213 that are in the vicinity of Q_B. Those separate redox potential values exhibit more information than the reaction energy of electron transfer. Alternatively, we also study the protonation state of Glu-L212 and Asp-L213 as a function of the charge state of the two quinones. This information can be used to gain more insight about the role of the protonation pattern of titratable groups on the mechanism of the electron transfer from Q_A and Q_B in the RC. Furthermore, we can gain more confidence in our results from electrostatic energy computations on quinone redox potentials and specific protonation pattern in RCs by comparing them with more detailed experimental data.

MATERIALS AND METHODS

Coordinates. For our computations, we used the light-exposed and dark-adapted crystal structures of the RC from *R. sphaeroides* at a resolution of 2.6 Å (PDB 1AIG) and 2.2 Å (PDB 1AIJ), respectively (*7*), and the structure of the double mutant E(L212)A and D(L213)A (AA mutant) of RC from *R. sphaeroides* (PDB 1K6N) (*59*). The atomic coordinates were prepared in the same way as in previous applications (*9*). Since there are no hydrogen atoms in the crystal structures, they were generated, and their positions were energetically optimized with CHARMM (*21*), while the positions of all non-hydrogen atoms were fixed and all titratable groups were kept in their standard charge state and the quinones in their oxidized neutral charge state. We are using the notion (protonation) charge state for a titratable molecular group if its atomic partial charges are fixed, while referring to protonation state comprises fluctuations of charges at a specific protonation probability of that group.

Generally, there is no explicit experimental information available on the position of the hydrogen atoms of water molecules found in the crystal structures of proteins. Generating these coordinates by modeling depends critically on the protonation pattern of titratable residues, and often more than one conformation is possible. To avoid this ambiguity, we did not treat water molecules explicitly. Hence, all water molecules in the crystal structures were removed. However, the effect of water molecules was considered implicitly by the high dielectric constant of the solvent used for the resulting cavities in the protein. There are a number of studies to evaluate electrostatic energies in protein−water systems based on solution of the linearized Poisson−Boltzmann equation (LPBE), which considered the influence of explicit water molecules. Generally, the agreement with experimental pK_a values of titratable groups (*22*) and of redox active cofactors (*23*) did not improve. On the other hand, we successfully explained pK_a values in myoglobin (*24*), redox potentials of hemes in cytochrome *b* (*25*), quinones in bacterial RCs (*9*, *26*), and tryptophans and

tyrosines in photolyase (*27*) without considering water molecules explicitly, which justifies the approach in the present study.

Atomic Partial Charges. Atomic partial charges of the amino acids were adopted from the all-atom CHARMM22 (*28*) parameter set. These atomic partial charges are more appropriate than charges from the CHARMm21.3 parameter set of Molecular Simulation Incorporated used in previous work (*9*), where nonpolar hydrogens were represented implicitly by extended atoms. Instead of attaching an explicit hydrogen atom on one of the oxygens of the protonated carboxyl group of glutamate or aspartate, the charges of these two oxygens were both increased symmetrically by +0.5 unit charges to account implicitly for the presence of the proton. A similar procedure was used for the basic groups of arginines and lysines, where instead of removing a proton explicitly in the deprotonated state the charges of all protons at the corresponding basic group were diminished symmetrically by a total unit charge. For cofactors and residues whose charge states are not provided in the CHARMM22 parameter set, the same atomic partial charges were used as in previous work (*9*). Controlled variations of the charge state of selected titratable groups as applied to Glu-L212, Asp-L213, and the two quinones were achieved by linear interpolation of the atomic partial charges of these molecular groups between the fully ionized (reduced) and fully protonated (oxidized) charge state.

Computation of Protonation Pattern and Redox Potentials. The computation of the energetics of protonation pattern is based on the electrostatic continuum model by solving the LPBE with the program MEAD from Bashford and Karplus (*29*). The ensemble of protonation patterns was sampled by a Monte Carlo (MC) method where we used our own program *Karlsberg* (*30*). The detailed procedure that we used is described in refs *9* and *26*. The dielectric constant was set at $\epsilon = 4$ inside the protein and $\epsilon = 80$ for water. Discussions about the appropriate choice of the dielectric constant for proteins can be found in refs *31*−*35*. All computations were performed at 300 K with pH 7 and an ionic strength of 100 mM. The LPBE was solved using a three-step grid-focusing procedure with a starting grid resolution of 2.5 Å, a second grid resolution of 1.0 Å, and a final grid resolution of 0.3 Å.

The MC sampling yields the probabilities $[A_{ox}]$ and $[A_{red}]$ for the charge states of the redox-active group *A*. With these probabilities, the redox potentials can be calculated from the Nernst equation for a one-electron couple

$$E = E^\circ + \frac{RT}{F}\ln\frac{[A_{ox}]}{[A_{red}]} \quad (1)$$

where *F* is the Faraday constant, *E* is the actual redox potential of group *A*, and E° is the standard redox potential. To minimize the statistical error in evaluating the redox potential from the Nernst eq 1, we applied a bias redox potential to the redox-active group *A* such that we have an equal amount of both redox states ($[A_{ox}] = [A_{red}]$). The resulting bias potential is just the value of the redox midpoint potential, which we calculated for the quinones in the A- and B-branch ($E_m(Q_A)$ and $E_m(Q_B)$). This also corresponds to a standard procedure to determine redox potentials experimentally by varying the solvent redox potential to observe an equal amount of the redox active group to be oxidized and reduced. Redox potentials that are determined in this way refer to a fixed protonation state of the surrounding titratable groups. To gain information on how the protonation pattern of titratable residues differs for specific redox states of cofactors, as for instance $Q_A^- Q_B^0$ or $Q_A^0 Q_B^-$, the redox states of these groups are fixed, while titrating all other residues.

The standard deviation in the protonation probability of a single titratable group estimated from the MC sampling procedure was much smaller than 0.01 protons. For each computation of protonation pattern, the sum of standard deviations of protonation probabilities from all titratable groups was about 0.02 protons, similarly as in former applications (*26*, *36*). The error in the electrostatic energy values resulting from a grid resolution of 0.3 Å that we used was estimated to be smaller than 10 meV (*36*).

The machinery to compute redox potentials of cofactors in proteins that we employed in the present application was used successfully before for a number of systems considering the redox potentials of heme (*25*) as well as tryptophan and tyrosine (*27*) in proteins. Since we did not treat water molecules explicitly in our electrostatic approach, water molecules were treated as not titratable, which is appropriate for pH values in a large regime extending from 1 to 13. As a consequence, the redox potential of quinone in solution possesses no pH dependence.

The reaction energy ΔG° of electron transfer from $Q_A^- Q_B$ to $Q_A Q_B^-$ can be obtained from the difference of the redox potentials $E_m(Q_A)$ and $E_m(Q_B)$ of the two quinones multiplied by the unit charge q_e as follows:

$$\Delta G^\circ(Q_A^- Q_B \rightarrow Q_A Q_B^-) = q_e[E_m(Q_A) - E_m(Q_B)] \quad (2)$$

Redox Potential of Ubiquinone in Solution. Measurements of the redox potential of ubiquinone in aqueous solution yield a value in the range of −100 to −120 mV (*37*) versus normal hydrogen electrode. A lower value of −230 mV was obtained in earlier work by using a rough estimate only (*38*). These values are artificially high because of an inevitable proton uptake by reduced quinone, which occurs in protic solvents. In aprotic solvents, protonation of reduced quinone is not possible yielding a much lower value of the redox potential of ubiquinone. We considered ubiquinone in dimethylformamide (DMF) with dielectric constant $\epsilon = 37$ as reference system where the ubiquinone redox potential was measured to be −360 mV (*39*), although the electrolyte whose presence is needed in DMF to measure redox potentials may influence this result. The redox potential of a quinone in protein environment was obtained by calculating the electrostatic energies of the quinone in the reference system and the protein environment and by adding the difference of these electrostatic energies to the experimental value of the redox potential in the reference system.

Redox Potentials of Quinones in RCs. The in situ redox potential of ubiquinone in the Q_A site was measured by redox titration of RCs from *R. sphaeroides* to be −50 mV pH independent in isolated RCs (*40*−*42*) or between +50 mV at low pH (*42*) and −180 mV at high pH in chromatophores (*4*, *43*, *44*) where the RC is imbedded in the light harvesting 1 (LH1) complex. However, in other measurements based on flash-induced production of SP^+, the redox potential of

Table 1: Protonation States of Glu-L212 and Asp-L213 in RC from *R. sphaeroides*

	$Q_A^-Q_B$		$Q_AQ_B^-$	
method	Glu-L212	Asp-L213	Glu-L212	Asp-L213
experimental				
photovoltage[a]	protonated		protonated	
kinetic study[b]		ionized		ionized
FTIR[c]	partially ionized	mostly ionized	protonated	mostly ionized
theoretical				
molecular dynamics[d]	ionized protonated	ionized ionized	protonated	protonated
electrostatic comp. 1[e]				
dark-adapted structure	mostly ionized	partially ionized	protonated	protonated
light-exposed structure	partially ionized	mostly ionized		
electrostatic comp. 2[f]	protonated	ionized	protonated	protonated

[a] See ref *54*. [b] See refs *18*−*20*. [c] See refs *14* and *16*. Proton uptake by Glu-L212 has been estimated to be 0.3−0.4 H^+ at pH 7. [d] See ref *17*. The results were derived by MD simulation starting from the crystal structure of Ermler et al. (*11*). Using fixed charge states with both Glu-L212 and Asp-L213 ionized or Glu-L212 protonated and Asp-L213 ionized, the structures obtained by MD simulation were quite similar to the dark-adapted structure (*7*). [e] See ref *9*. Protonation probabilities of Glu-L212 and Asp-L213 in the state $Q_A^-Q_B^0$ are 0.27 and 0.75 in the dark-adapted structure and 0.81 and 0.37 in the light-exposed structure, respectively. [f] See ref *10*. Proton uptakes by Asp-L210 and Asp-L213 were involved in the conformational change from the dark-adapted structure to the light-exposed one, whereas no proton uptake by Glu-L212 was observed.

Q_A was found to be pH dependent also in isolated RCs. The measured values varied between −200 and −100 mV at pH 10 and −100 and 0 mV at pH 8.1 (*45*), similar to the pH dependence observed in chromatophores (*4*, *43*, *44*). More recent studies of proton uptake of the RC going along with Q_A reduction that are based on delayed fluorescence measurements clearly demonstrated the pH dependence of the redox potential of Q_A also in isolated RC (*46*). Reaction energies of the electron transfer from Q_A to Q_B estimated by the charge recombination rate in different labs vary from −52 to −78 meV (*4*, *47*−*49*). Combining these values with the range of measured in situ redox potentials for $E_m(Q_A)$, we can conclude that the value of $E_m(Q_B)$ is in the range from 0 to +30 mV or −130 to −100 mV for the in situ redox potential $E_m(Q_A)$ of −50 and −180 mV, respectively. Note that the crystal structures obtained under light-exposed conditions refer to continuous illumination, whereas the measurements on the reaction rate of the electron transfer from Q_A to Q_B may refer to different conditions of illumination that can have an influence on the measured redox potentials.

Interestingly, the slope of the pH dependence of $E_m(Q_A)$ in chromatophores adopts the value −60 mV/pH, which is typical for a proton uptake coupled redox reaction in solution according to Nernst law. At high pH values corresponding to low values of the redox potential of Q_A in both chromatophores and isolated RCs, the degree of proton uptake going along with the formation of Q_A^- is likely to be small. The pH dependent proton uptake may also go along with subtle conformational changes that occur in the redox state Q_A^-.

The proton uptake process of RCs is likely to be much slower than the time scale needed for the actual electron-transfer process from $Q_A^-Q_B$ to $Q_AQ_B^-$ (*40*, *50*). Hence, Arata et al. (*4*, *43*) assumed that the proton uptake by the RC after formation of Q_A^- is only partially accomplished before the electron is transferred from Q_A to Q_B. This effectively corresponds to a higher pH value in the neighborhood of Q_A. Therefore, the appropriate value of the effective redox potential $E_m(Q_A)$ relevant for the electron-transfer process from Q_A to Q_B was assumed to be −180 mV, corresponding to the lowest measured redox potential of Q_A obtained at high pH (*4*, *43*, *44*). Interestingly, the redox potential of Q_A is shifted to a considerably higher value of +160 mV in isolated RCs if Q_B is lacking (*51*). Within the above framework this can be understood since in the absence of Q_B the Q_A^- redox state has ample time to equilibrate with respect to conformation and protonation states.

In the light-exposed structure, the carbonyl oxygen of Q_B distal from the non-heme iron forms simultaneous three branched hydrogen bonds with the amide nitrogen of Ile-L224 (N−O distance 3.0 Å) and Gly-L225 (N−O distance 3.3 Å) and the OH group of Ser-L223 (O−O distance 3.2 Å), while the proximal carbonyl oxygen of Q_B forms a single strong hydrogen bond with the Nδ nitrogen of His-L190 (N−O distance 2.8 Å) (*7*). In the dark-adapted structure, only a single hydrogen bond from the amide backbone of Ile-L224 to the distal carbonyl oxygen of Q_B (N−O distance 3.1 Å) was observed (*7*, *11*). Hydrogen bond interaction with the carbonyl oxygens of the ubiquinone is likely to stabilize the redox state Q_B^-, thus raising the value of the redox potential $E_m(Q_B)$ (*52*). As a consequence, the redox state $Q_A^0Q_B^-$ is stabilized more in the light-exposed than in the dark-adapted structure (*8*, *9*) rendering the electron transfer from Q_A to Q_B downhill in energy for the light-exposed structure only.

Density functional theory calculations of quinones in photosystem I suggested that one strong hydrogen bond with one carbonyl oxygen atom of the phylloquinone can account for an increase in redox potential of about 250 mV (*53*). Interestingly, this value is of the same magnitude as the estimated shift of $E_m(Q_B)$ from the solution value of −360 mV to values between −130 and −100 mV that are estimated by assuming that the redox potential of Q_A corresponds to the lowest measured value of −180 mV obtained at high pH.

Protonation States of Glu-L212 and Asp-L213. Table 1 summarizes experimental and theoretical results on the protonation state of the two key residues Glu-L212 and Asp-L213 for the electron transfer from Q_A to Q_B. Agreement on the protonation state of those two residues was reached (i) for Asp-L213 in the state $Q_A^-Q_B^0$ where it is considered to be ionized and (ii) for Glu-L212 in the state $Q_A^0Q_B^-$ where it is found to be protonated (see Table 1).

Regarding proton uptake by Glu-L212 and Asp-L213 with the formation of Q_B^-, no agreement has been reached yet. The light-induced photovoltage changes upon formation of Q_B^- indicated that Glu-L212 contributes to proton uptake only at high pH and that it remains essentially protonated at pH 7 in both redox states $Q_A^-Q_B^0$ and $Q_A^0Q_B^-$ (*54*). From FTIR difference spectroscopy on mutated RCs it was concluded that Glu-L212 participates in the reduction of Q_B with a fractional proton uptake by 0.3−0.4 H^+ at pH 7 (*14*, *15*). Kinetic studies (*18*−*20*) and FTIR spectroscopy (*14*, *15*) suggested no proton uptake by Asp-L213, although MD simulations have conversely implied proton uptake by this residue (*17*). Electrostatic energy computations with a continuum solvation model showed different results, too (*9*, *10*). In one study with no explicit water, it was found that the main protonation changes occur at both residues, Glu-L212 and Asp-L213 (*9*). In another study, where selective explicit water molecules were considered to describe the protonation pattern in RCs, a proton uptake by Asp-L210 and Asp-L213 was observed (*10*), whereas no evidence for proton uptake by Asp-L210 was found in FTIR studies (*55*).

RESULTS AND DISCUSSION

Computed Redox Potentials of the Quinones in the Light-Exposed Structure Influenced by the Charge States of Glu-L212 and Asp-L213. The dependence of the redox potential of the ubiquinones on the protonation charge state of Glu-L212 and Asp-L213 at pH 7 was investigated by varying the net charges of these two acidic residues, while the charge states of all other titratable residues were allowed to fluctuate during the titration procedure (Figure 2). Accordingly, we calculated the value of $E_m(Q_A)$ as a function of the protonation charge state of Asp-L213 with Q_B in the neutral charge state while constraining the net charge of Glu-L212 at three different values to be fully protonated (1.0) and partially protonated (0.6 and 0.8). In the same way, we monitored the redox potential $E_m(Q_B)$ as a function of the protonation charge state of Asp-L213 with Q_A in the neutral charge state while constraining Glu-L212 to be fully (1.0) and partially protonated (0.6 and 0.8). The charge state of Glu-L212 was varied only in this limited range since all known experimental data (*14*, *16*, *54*) exclude a mainly ionized Glu-L212 in the redox state $Q_A^-Q_B^0$, while the protonation state of Asp-L213 is less definite, and therefore, its charge state is varied over the whole range.

Considering Glu-L212 to be fully protonated in the redox state $Q_A^0Q_B^-$ agrees with experimental findings (see Table 1). In the present computations, we found that Glu-L212 should only be partially protonated at 0.6 H^+ rather than 0.8 H^+ in the redox state $Q_A^-Q_B^0$ to obtain agreement with the measured redox potential for Q_A of −180 mV (see Figure 2).

Constraining Glu-L212 and Asp-L213 to be fully protonated in the redox state $Q_A^0Q_B^-$ yields a downhill reaction energy of −70 meV for the electron transfer from Q_A to Q_B. But, if Glu-L212 is only partially protonated by 0.8 H^+ (0.6 H^+), the redox potential $E_m(Q_B)$ shifts down by about 60 mV (120 mV) as compared to value for fully protonated Glu-L212, regardless of the protonation charge state of Asp-L213 (Figure 2). As a consequence, the electron transfer from Q_A to Q_B becomes isoenergetic (or even uphill) and no longer

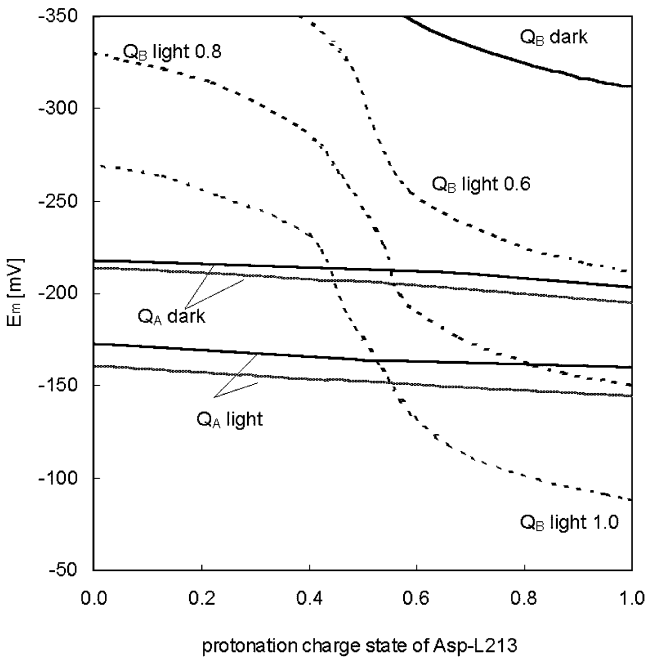

FIGURE 2: Dependence of quinone redox potentials of RC from *R. sphaeroides* on protonation charge state of Asp-L213 that varies from zero to full protonation. Results are shown for light-exposed (light) and dark-adapted (dark) structures at pH 7. The solid (dashed) lines depict the redox potential dependence of Q_A (Q_B). For the redox potential of Q_A, the protonation charge state of Glu-L212 was fixed to be at 0.6 protons (upper curve) and 0.8 protons (lower curve). For Q_B in the dark-adapted (dark) structure, the protonation charge state of Glu-L212 was fixed to be at 1.0. For Q_B in the light-exposed structure (dashed lines), the protonation charge state of Glu-L212 was fixed to be at 0.6 protons (upper curve), 0.8 protons (middle curve), and 1.0 protons (lower curve).

downhill in energy. Hence, it is necessary that Glu-L212 is almost fully protonated in the redox state $Q_A^0Q_B^-$ to render the first electron transfer from Q_A to Q_B downhill in energy. That is in full agreement with the FTIR measurements.

If the charge state of Asp-L213 is varied from fully ionized to protonated and the charge state of Glu-L212 is fixed at 0.6 H^+ (0.8 H^+), the redox potential $E_m(Q_A)$ increases from −173 to −160 mV (−161 to −144 mV) only. The calculated values of $E_m(Q_A)$ corroborate with the measured redox potential of −180 mV obtained for chromatophores at high pH (*4*, *43*, *44*) and with the values between −200 and −100 mV at pH 10 in isolated RCs (*45*). Since we take the same (light-exposed) structure with oxidized Q_A^0 to compute both redox states of Q_A, we neglect subtle conformational changes that may be coupled to proton uptake by the RC and occur with a transition to the reduced state Q_A^-. As a result of these computational constraints, the stabilization of the reduced state Q_A^- is underestimated in our computations resulting in a redox potential whose value is lower than under equilibrium conditions where the reduced state Q_A^- is fully relaxed. This effect also occurs if the electron is transferred from Q_A to Q_B fast enough to avoid these conformational changes. The same may be true for the measured values of the redox potential of Q_A at high pH, where proton uptake may be reduced. Note that proton uptake of the RC going along with a reduction of Q_A is mainly due to electrostatic interactions with the acidic cluster close to Q_B (*56*−*60*).

Our computational results for $E_m(Q_B)$ indicate that Asp-L213 should be mainly protonated in the Q_B^- state to render

the redox potential $E_m(Q_B)$ larger than $E_m(Q_A)$, which is needed to guarantee that the electron transfer from Q_A to Q_B is energetically downhill. A protonated Asp-L213 in the Q_B^- state is in agreement with results from MD simulations where it was concluded that Asp-L213 must be protonated before the conformational change from the dark-adapted to the light-exposed structure can occur (*17*). Our results suggest that any protonation charge state of Asp-L213 above 0.6, which guarantees that the electron transfer from Q_A to Q_B is energetically downhill, is acceptable (Figure 2). Since the dependence of the computed redox potential of Q_A on the protonation charge state of Asp-213 is small, a protonation charge state of Asp-L213, which is lower for the initial $Q_A^-Q_B$ than for the final state $Q_AQ_B^-$, would also render the electron-transfer reaction to be downhill in energy. But it would not agree with results from FTIR spectra (*14*, *16*) and kinetic studies (*18*−*20*) where no proton uptake at Asp-213 was observed.

On the basis of these computations, the protonation charge state of Asp-L213 is estimated to be about 0.75−1.0 in the redox state Q_A^0 to satisfy the experimental value of $E_m(Q_B)$. From our computations of $E_m(Q_A)$ in the redox state Q_B^0, no clear restrictions can be derived with respect to the protonation charge state of Glu-L212 and Asp-L213. However, the calculated redox potential $E_m(Q_A)$ agreed better with the experimental data considering a protonation charge state of 0.6 instead of 0.8 for Glu-L212. This is also in agreement with FTIR results, where at Glu-L212 a proton uptake of 0.3−0.4 H^+ was found going along with the electron transfer (*14*, *16*). Assuming that no proton uptake occurs at Asp-L213, the reaction energy of electron transfer is according to our computation between −50 and −70 meV for a protonation charge state of Asp-L213 between 0.75 and 1.0, respectively. If for instance the protonation charge state of Asp-L213 is at 0.8 H^+ in the initial and final state of electron transfer from Q_A to Q_B and there is a proton uptake of 0.4 H^+ at Glu-L212, the computed values of the redox potentials $E_m(Q_A)$ and $E_m(Q_B)$ are −160 and −100 mV, respectively. The electron-transfer energy calculated from the difference of the in situ redox potentials of the quinones is −60 meV, which is also in good agreement with the experimental values, particularly if one compares it with the value of −67 meV measured between pH 6 and 8.5 (*48*).

Protonation States of Glu-L212 and Asp-L213 as a Function of the Redox Charge States of the Quinones. The redox potential of Q_B is determined as the redox potential of the external solvent that provides an equal amount of Q_B^0 and Q_B^-. Under these conditions, we cannot obtain the protonation pattern for the limiting situations where Q_B is fully oxidized or reduced. To achieve that, we alternatively investigated the dependence of the protonation states of all titratable residues in RC on the charge states of Q_A and Q_B by shifting the negative unit charge continuously from Q_A to Q_B while fixing the total charge at both quinones to equal a negative unit charge. With this procedure that models the electron-transfer reaction from Q_A to Q_B, significant changes of the protonation states were found for Glu-L212, Asp-L213, and Asp-M17 only (Figure 3). This justifies the present study, which is focused on the protonation charge states of Glu-L212 and Asp-L213 to investigate their influence on the quinone redox potentials. Note that for the computed results exhibited in Figure 3 no constraining conditions were employed for the charge states of all titratable residues in the RC except for the two quinones. While shifting the negative charge from Q_A to Q_B, the protonation of Asp-L213 (Asp-M17) changes only moderately from 0.9 to 1.0 (0.0 to 0.1). But at the same time, the protonation state of Glu-L212 varies considerably from 0.15 to 1.0. This is partially in agreement with FTIR spectroscopy, where it was found that Glu-L212 changes its protonation state from 0.6 to 1.0, while Asp-L213 does not change its protonation state but remains unprotonated in contrast to our computations (*14*, *16*).

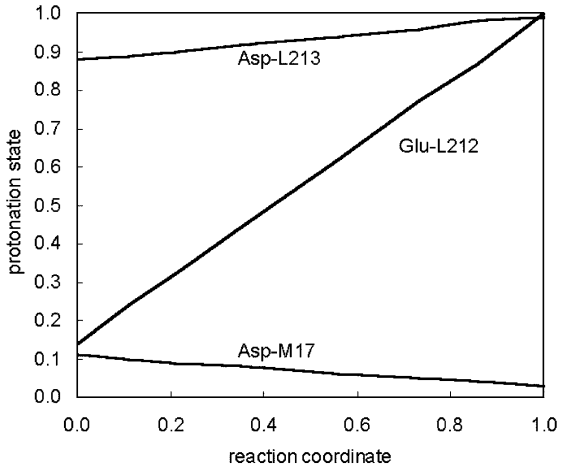

FIGURE 3: Protonation state of Asp-L213, Glu-L212, and Asp-M17 as a function of the charge state of the two quinones. The reaction coordinate varies from zero corresponding to the charge state $Q_A^-Q_B$ and unity corresponding to the charge state $Q_AQ_B^-$. The intermediate values of the reaction coordinate correspond to fractional charges at the two quinones, which sum up to a unit negative charge. In this computation, the charge states of the quinones were varied deterministically, while all other residues including Asp-L213, Glu-L212, and Asp-M17 were titrated.

Comparison of $E_m(Q_A)$ in Light-Exposed and Dark-Adapted Structure, a Functional Link between Q_A and Q_B. In the light-exposed structure, the redox potential $E_m(Q_A)$ is about 50 mV higher than in the dark-adapted structure. This increase of the redox potential $E_m(Q_A)$ would lead to a corresponding decrease of the driving force of the electron-transfer reaction if the redox potential $E_m(Q_B)$ would not change as well. However, the corresponding upshift in the redox potential of Q_B is about 200 mV, which is considerably larger than that of Q_A. As a consequence, if Asp-L213 is fully protonated in the Q_B^- state, the calculated reaction energy of the electron transfer from Q_A to Q_B decreases from about +110 meV in the dark-adapted structure to −70 meV in the light-exposed structure, yielding a net positive driving force for the electron transfer in the light-exposed structure.

The increase of the redox potential $E_m(Q_A)$ between the dark-adapted and the light-exposed structure is mostly due to the interaction of Q_A with Q_B and with Glu-L212 and other acidic residues close to Q_B. However, the strength of the electrostatic interaction of Glu-L212 with Q_A is smaller than with Q_B since Glu-L212 is much closer to Q_B than to Q_A with distances of about 5 and 15 Å, respectively (*61*). It remains to be clarified whether the difference in the interaction of Glu-212 with Q_A between the dark-adapted and the light-exposed structure is related to direct electrostatic interactions between Q_A and Glu-L212 or an indirect interaction. The latter type of interaction would be mediated by titratable residues whose protonation probabilities vary

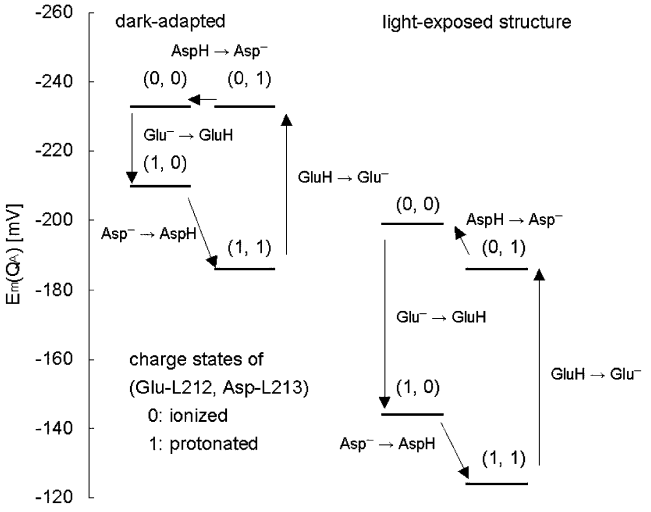

FIGURE 4: Variation of the redox potential of Q_A with proton uptake by Glu-L212/Asp-L213 simulated at pH 7.

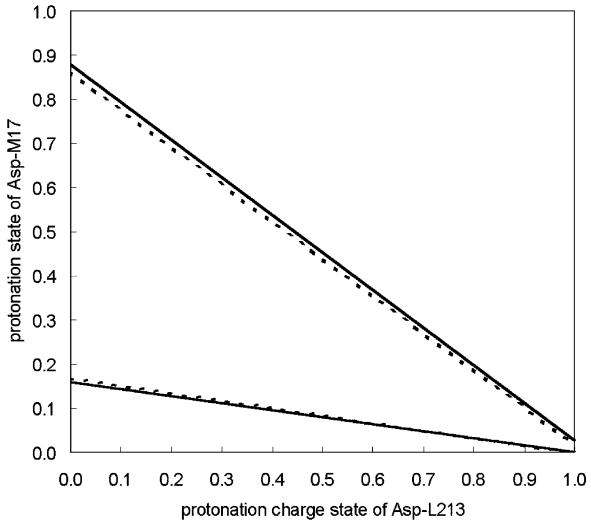

FIGURE 5: Correlation of the protonation state of Asp-M17 with Asp-L213 in the light-adapted structure (upper line) and the dark-adapted structure (lower line) at pH 7. The protonation charge state of Asp-L213 was varied as in Figure 2, with Glu-L212 fixed at its fully protonated charge state in the redox states $Q_A^-Q_B^-$ (solid line) and $Q_A^0Q_B^-$ (dashed line).

by changing the protonation charge state of Glu-L212. In our computations, no significant change of protonation pattern occurred by changing the protonation charge state of Glu-L212 from 0.6 to 0.8.

To quantify the amount of direct electrostatic interactions between Glu-L212 and Q_A in the dark-adapted and light-exposed structures, we computed the change in $E_m(Q_A)$ by varying only the protonation charge state of Glu-L212 between 0.6 and 0.8 in the dielectric environment of the RC, while all atomic partial charges in the RC except for Glu-L212 and Q_A were set to zero. As a result of these computations, we obtained a shift in the redox potential of Q_A between the two charge states of Glu-L212, which is the same for the dark-adapted and the light-exposed structure, namely 13 mV. Since our computations with variable titratable groups provided values of the redox potential of Q_A, which exhibited a different albeit small shift by varying the charge state of Glu-L212 between the dark-adapted and the light-exposed structure (see Figure 2), an indirect electrostatic interaction must be present as well.

The above-described interaction of Glu-L212 with Q_A is in agreement with a study of the pH dependence of the free energy of the state $SP^+Q_A^-$ (*46*). There it was found by pH titration that the redox potential of Q_A increases by about 50 mV upon proton uptake at Glu-L212 and other residues from the acidic cluster at Q_B. This indicates that the interaction energy between the titratable groups around Glu-L212 and Q_A is about 50 meV providing a functional link between the Q_A and the Q_B sites (*37*). However, since the distance between Q_A and Q_B is large (~17 Å), influences other than these electrostatic interactions were also considered, as for instance, interactions with the non-heme iron complex (*46*).

In the light-exposed structure, we found $E_m(Q_A)$ to increase by about 50 mV, independent of the charge state of Asp-L213 if the protonation of Glu-L212 increased from completely ionized to fully protonated while all other residues in our computation were titrated (Figure 4). These results corroborate experimental observations on the reaction energy of charge recombination between oxidized SP and Q_A^- from which it was concluded that the value of $E_m(Q_A)$ is not sensitive to the charge state of acidic residues other than Glu-L212 (*46*). In the dark-adapted structure, the same shift of $E_m(Q_A)$ was obtained with Asp-L213 fully protonated, while all other residues in our computation were titrated, whereas for ionized Asp-L213 the calculated shift of $E_m(Q_A)$ was only 23 mV (Figure 4). Also, in the dark-adapted structure with ionized Glu-L212, the $E_m(Q_A)$ did not change upon proton uptake by Asp-L213. The largest dependence of $E_m(Q_A)$ on the protonation of Asp-L213 was observed in the dark-adapted structure with fully protonated Glu-L212 (Figure 4).

The insensitivity of $E_m(Q_A)$ on the protonation of Asp-L213 might be due to charge compensation by the strong coupling of the protonation states of Asp-L213 and Asp-M17. The coupling is stronger in the light-exposed than in the dark-adapted structure, although the effect on $E_m(Q_A)$ in the presence of protonated Glu-L212 appears only by 4 mV larger change upon the protonation process of Asp-L213 in the dark-adapted structure than the light-exposed structure. In the light-exposed structure, we found that Asp-M17 is fully ionized (protonated with 0.86−0.88 H^+) if Asp-L213 is fully protonated (fully ionized). Note that the charge state of Q_A has practically no influence on the correlation of the protonation of Asp-L213 and Asp-M17 (Figure 5).

Comparison of $E_m(Q_B)$ in Light-Exposed and Dark-Adapted Structure. Here we like to investigate the factors that lead to a different redox potential of Q_B in the light-exposed and the dark-adapted RC at pH 7 while Glu-L212 and Asp-L213 are fully protonated. In the dark-adapted structure, the value of $E_m(Q_B)$ is less than −300 mV. Interestingly, this value is close to the redox potential value of −360 mV measured for ubiquinone in DMF that is used as reference system for our computations. If both Glu-L212 and Asp-L213 are fully protonated, the redox potential of Q_B is −88 mV in the light-exposed structure that is 224 mV higher than in the dark-adapted structure (Table 2).

One may speculate that the correlation of the redox potential of Q_B in the dark-adapted RC with the DMF solution value is due to the presence of cavities and water

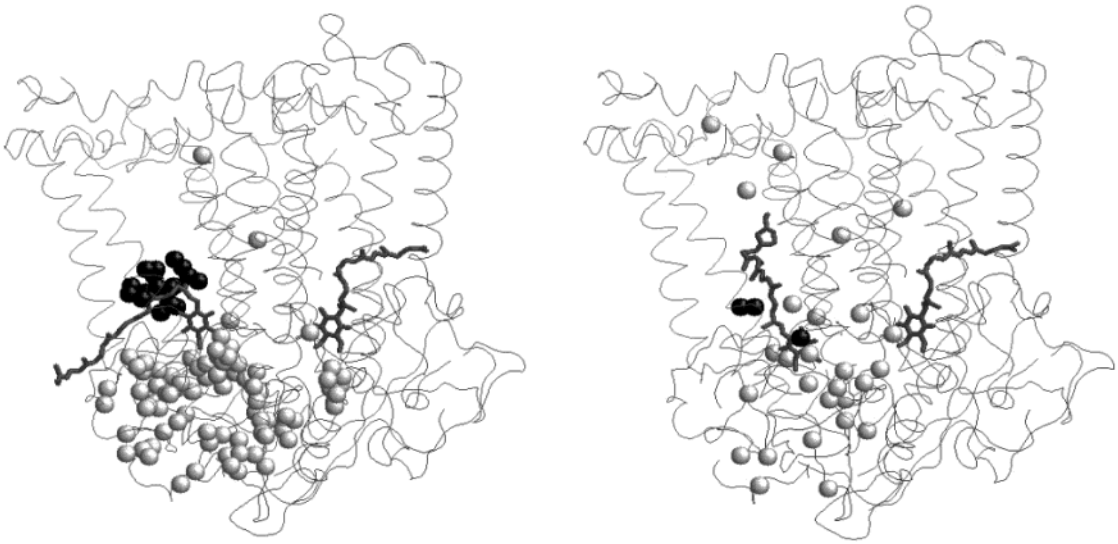

FIGURE 6: Locations of water molecules around Q_B in the dark-adapted (left) and light-exposed (right) structure. Quinone Q_B is situated on the left side in both of the structures. The oxygen atoms of crystal (artificially added) water molecules within the distance of 20 Å (10 Å) from the Q_B ring atoms are displayed in white (black) spheres. There are 82 (*27*) crystal waters selected in the dark-adapted (light-exposed) structure and 18 (*3*) could be added in the dark-adapted (light-exposed) structure.

Table 2: Factors Determining the Difference in the Redox Potential of Q_B between Light-Exposed (Light) and Dark-Adapted (Dark) Structure[a]

	$E_m(Q_B)$ [mV]		
	dark	light	Δ(light − dark)
wild type	−312	−88	224
zero charge of imidazole from His-L190	−375	−270	105
zero charge of Fe	−398	−253	145
zero charge of His-L190 and Fe	−461	−435	26

[a] Computations were done at pH 7 with fully protonated Glu-L212 and Asp-L213. Note that in the last column, Δ(light − dark), the sum of the first and last term equals the sum of the second and third term demonstrating the additivity of energies computed in the frame of LPBE.

molecules near Q_B. This is corroborated by the fact that there are many more water molecules found in the dark-adapted than in the light-exposed crystal structure of the RC (Figure 6). However, the excess of water molecules in the dark-adapted crystal structure may also be explained by the higher resolution, which is 2.2 Å for the dark-adapted and 2.6 Å for the light-adapted structure. The latter value may be too low to find all water molecules. Therefore, we checked both crystal structures for additional cavities in the neighborhood of Q_B that are not filled with crystal water by adding extra water molecules within a distance of at most 10 Å from any of the quinone Q_B ring atoms using an overlay technique similarly as done before (*62*). As a result, we succeeded in adding 18 water molecules in the dark-adapted structure, while only three additional water molecules were fitted in the light-adapted crystal structure. Except for one water molecule in the light-adapted structure, all of these additional water molecules were placed near to the surface of the RC at the end of the exit channel through which the quinone Q_B is expected to move out of the pocket as dihydroquinone Q_BH_2 (see Figure 6). This clearly demonstrates that there are only small cavities close to quinone Q_B in the light-adapted structure, whereas a larger cavity appears in the dark-adapted structure where additional water molecules would fit.

As explained in Materials and Methods, all water molecules were removed in our computations of electrostatic energies. Their influence was taken into account implicitly since in cavities appearing after removing the water molecules the dielectric constant was set to 80. To check whether the redox potential of Q_B adopts a lower value in the dark-adapted than in the light-exposed structure because of the larger exposure to water located in the cavities, we computed the redox potential of Q_B in the dark-adapted structure setting the dielectric constant in the volume covered by crystal and extra water molecules at $\epsilon = 4$, which is the same value used for the interior of the protein. The atomic partial charges of the water molecules were set to zero. Surprisingly, we observed a downshift of the redox potential of Q_B by only 7 mV in the presence of fully protonated Glu-L212 and Asp-L213. Hence, differences in the interaction of Q_B with water in nearby cavities cannot explain the shift in the redox potential between the dark-adapted and the light-exposed structure.

The oxygen atom of Q_B distal to the non-heme iron is involved in hydrogen bonds in both the dark-adapted and the light-exposed structure. In the light-exposed structure, the oxygen atom of Q_B proximal to the non-heme iron forms a hydrogen bond with the His-L190 that ligates with the non-heme iron. This hydrogen bond is absent in the dark-adapted structure. The positively charged iron that polarizes the imidazole ring of His-L190 strengthens the hydrogen bond leading to an upshift of the redox potential $E_m(Q_B)$. The influence of the hydrogen bonding on the redox potential of Q_B was investigated by turning off the atomic charges of the imidazole ring of His-L190 in both (light-exposed and dark-adapted) structures while keeping the low dielectric constant of $\epsilon = 4$ in the volume covered by these atoms. As a consequence, the difference in the computed redox potentials of Q_B was reduced from 224 to 105 mV (Table 2). Alternatively, by turning off the atomic charges of the non-heme iron, the difference in the redox potentials of Q_B

decreased to the new value of 145 mV. The influence from His-L190 and non-heme iron is additive (Table 2). Turning off the charges of both components yields a downshift of the redox potential of Q_B in the light-exposed and dark-adapted structure leading to a difference in the redox potential that is reduced to 26 mV. In conclusion, the difference in redox potential of Q_B between the light-exposed and the dark-adapted structure is due to the influence from the hydrogen bond with His-L190 and the shorter distance between Q_B and the non-heme iron, which is 6.7 Å (10.5 Å) between the proximal oxygen of Q_B and the non-heme iron in the light-exposed (dark-adapted) structure.

Effects of Mutations of Glu-L212 and Asp-L213 to Ala on the Quinone Redox Potentials. In the double mutant E(L212)A and D(L213)A (AA mutant) of RC from *R. capsulatus*, the first electron transfer from Q_A to Q_B occurs, but the photocycle is interrupted at this point (*63*) presumably since the quinone cannot be protonated because of the lack of the side chains of Glu-L212 and Asp-L213. Recently, the crystal structure of the AA mutant in the RC from *R. sphaeroides* was solved revealing an expanded Q_B cavity that is larger than one would expect just from a replacement of the side chains of Glu-L212 and Asp-L213 by Ala (*64*). In the AA mutant structure, the carbonyl oxygen of Q_B distal to the non-heme iron forms only a single hydrogen bond with the amide nitrogen of Ile-L224 (N−O distance 2.9 Å) instead of the 3-fold hydrogen bond in the wild-type RC. The hydrogen bond of the proximal carbonyl oxygen of Q_B with the Nδ nitrogen of His-L190 is considerably weaker than in the wild-type RC (N−O distance of 3.3 Å in the AA mutant instead of 2.8 Å in the wild type). The same is the case for the corresponding hydrogen bond of Q_A with His-M219 changing its lengths from 2.9 Å in the wild type to 3.2 Å in the AA mutant RC. Although the structure of the AA mutant RC was obtained under dark-adapted conditions, Q_B is located in a proximal position with respect to the non-heme iron as it is for the light-exposed structure of the native RC (*7*). Furthermore, the chain segment of residues L207−L213 is displaced by 0.5 Å and of residues L223−L227 by 0.3−0.7 Å with respect to the native RC.

We calculated the redox potential in the AA mutant crystal structure from *R. sphaeroides* (PDB 1K6N) (*59*) for Q_A and Q_B to be −276 and −200 mV, respectively. These redox potentials are for both quinones Q_A and Q_B in the AA mutant RC by about 100 mV more negative than in the light-exposed structure of the wild type RC. A major reason for the downshift in the redox potentials is the weakening of the hydrogen bond of the carbonyl oxygen proximal to the non-heme iron. The redox potential difference of the two quinones is with 76 mV only slightly larger than in the light-exposed structure of wild-type RC. This result corroborates kinetic studies of pH dependence, which led to the conclusion that the redox potential difference between Q_A and Q_B is larger in the AA mutant RC than in the native RC from *R. capsulatus* (*65*).

The most significant change in the protonation pattern of residues close to the quinones refers to Glu-M236, which is always (in all quinone redox states) protonated in the wild-type RC and always deprotonated in the AA mutant RC. Calculating the redox potentials of the quinones in the AA mutant RC with Glu-M236 constraint to be protonated while titrating all other residues, the contribution of the deprotonated Glu-M236 to the downshift of the redox potentials was estimated to be 20 mV for Q_A and 30 mV for Q_B.

Note that although the AA mutant crystal structure was obtained under dark-adapted conditions, the electron transfer is downhill in energy as opposed to the wild-type RC under the same conditions. Hence, it may be concluded that the conformational changes occurring in the AA mutant compensate for uphill reaction energy in the dark-adapted structure. In contrast to the wild-type RC, no significant change of the protonation pattern was observed upon the formation of Q_A^- or Q_B^-. To check this more carefully, we modeled an AA mutant structure by replacing the side chains of both Glu-L212 and Asp-L213 by Ala using the dark-adapted (light-exposed) wild-type structure. Thereby, we ignored the conformational changes occurring in the AA mutant structure. The redox potentials calculated for the modeled AA mutants are in the dark-adapted (light-exposed) structure −192 and −333 mV (−120 and −112 mV) for Q_A and Q_B, respectively. For the dark-adapted structure of the modeled AA mutant, these calculated values are close to the corresponding values of the dark-adapted structure from the wild-type RC. For the light-exposed structure of the modeled AA mutant, the reaction energy of electron transfer is now only marginally downhill in energy, and the value of $E_m(Q_B)$ [$E_m(Q_A)$] differs by 24 mV (53 mV) from the corresponding values of the wild-type RC with Glu-L212 fully protonated (protonation charge state of Glu-L212 at 0.6) and Asp-L213 fully protonated.

Proton Uptake at Q_B. Besides the role of Glu-L212 and Asp-L213, it is also worthwhile to consider the protonation state of the acidic cluster composed of six carbonic acids in the vicinity of Q_B (*66*) in connection with the proton transfer to Q_B that is connected with the electron transfer between the quinones (Figure 1). This cluster consists of Asp-L210, Asp-M17, Asp-H124, Asp-H170, Glu-H173, and Asp-L213. These acidic residues have been suggested to be involved in rapid proton-coupled electron transfer to Q_B (*67*−*70*). In a description of the pathway for the first proton transfer to Q_B, it was proposed that the proton is transferred via Asp-M17, Asp-L210, Asp-L213, and Ser-L223 (*71*) to the distal carbonyl oxygen of the quinone. In our study, Glu-H173 did not change its protonation state upon formation of Q_B^- but remained fully protonated ,while the charge states of Glu-L212 and Asp-L213 were varied extensively. This supports results from FTIR studies combined with data from site-directed mutations at Glu-H173 (*14*, *16*).

Asp-L210 and Asp-M17 play an important role in the proton transfer to the Q_B site, and it has been proposed that they act parallel in the proton-transfer chain to achieve an efficient proton uptake of Q_B^- (*72*, *73*). In our computation, we did not see any significant change of protonation at Asp-L210 and Asp-M17 upon formation of Q_B^-. Asp-L210 was ionized in both redox states of Q_B, whereas the protonation state of Asp-M17 depends on Asp-L213 and is ionized if Asp-L213 is protonated. But, even if Asp-L213 is fully ionized, Asp-M17 is not able to reach the fully protonated state (Figure 5). This result is consistent with FTIR spectra on point-mutated RCs that showed at least partially ionized

charge states of these two residues around pH 7 and no changes of their charge states upon formation of Q_B^- (*55*). During the variation of the charge states at Glu-L212 and Asp-L213 in the Q_B^- state, Asp-L210 was found to be fully ionized in our computation, regardless of the charge states of Glu-L212, Asp-L213, and Asp-M17. The protonation state of Asp-M17, however, exhibited a strong coupling with the protonation of Asp-L213 but not with any other titratable residue regardless of the protonation of Glu-L212. This coupling is demonstrated in Figure 5 for fully protonated Glu-L212, which corresponds to the situation just before the uptake of the first proton by the reduced Q_B^- (*74*).

CONCLUSION

The in situ absolute redox potentials of the quinones in the RC from *R. sphaeroides* were calculated by solving the LPBE and compared with experimental data. We investigated the influence of the charge states of the residues Glu-L212 and Asp-L213 in the vicinity of Q_B on the redox behavior of Q_A and Q_B. In our computations, the absolute value of the redox potential of Q_A was found to be between −173 and −160 mV, which agrees with the lowest values of the redox potential measured for Q_A in RC from *R. sphaeroides*. This low value may relate to conditions where the protonation pattern and conformation of the RC has no time to adjust to the reduced state Q_A^-. That is fulfilled for intact RCs where the electron is transferred from Q_A to Q_B before significant proton uptake may occur.

The redox potential of Q_A showed little dependence on the charge states of Asp-L213 in both the light-exposed and the dark-adapted structures. The redox potential of Q_B exhibits a strong dependence on the charge states of Glu-L212 and Asp-L213. Especially in the light-exposed structure, there is a dramatic shift of the redox potential by about 180 mV at pH 7, while the charge state of Asp-L213 is changed in the presence of a fully protonated Glu-L212. The lack of the hydrogen bond of Q_B with His-L190 and the larger distance of Q_B from the non-heme iron in the dark-adapted structure shifts the redox potential of Q_B to a value close to the redox potential of ubiquinone in DMF used as a reference system. This explains the discrepancy of $E_m(Q_B)$ between the dark-adapted and the light-exposed structure, too.

The value of the redox potential $E_m(Q_A)$ agrees better with the experimental value of the in situ redox potential when the protonation charge state of Glu-L212 is taken to be 0.6 H^+ than with a larger protonation. To obtain agreement with the measured value of $E_m(Q_B)$ and the reaction energy of the electron transfer from Q_A to Q_B, the protonation charge state of Asp-L213 has to be between 0.75 and 1.0, and Glu-L212 should be fully protonated. The calculated protonation pattern of Glu-L212 is in agreement with results obtained from FTIR spectroscopy and kinetic studies. In our computations, Asp-L213 was found to be nearly protonated, and there was no need to change its charge state by varying the redox state of the quinones. Hence, there is no proton uptake at this residue in agreement with the results from FTIR spectroscopy and kinetic studies, although from these measurements it was concluded that Asp-L213 should be fully ionized rather than protonated as found in our computations.

ACKNOWLEDGMENT

We thank Drs. Donald Bashford and Martin Karplus for providing the programs MEAD and CHARMM, respectively, and Dr. Björn Rabenstein for useful discussions.

REFERENCES

1. Lin, S., Katilius, E., Haffa, A. L. M., Taguchi, A. K. W., and Woodbury, N. W. (2001) *Biochemistry 40*, 13767−13773.
2. McElroy, J. D., Mauzerall, D. C., and Feher, G. (1974) *Biochim. Biophys. Acta 333*, 261−277.
3. Arata, H., and Parson, W. W. (1981) *Biochim. Biophys. Acta 636*, 70−81.
4. Arata, H., and Parson, W. W. (1981) *Biochim. Biophys. Acta 638*, 201−209.
5. Kleinfeld, D., Okamura, M. Y., and Feher, G. (1984) *Biochemistry 23*, 5780−5786.
6. Nabedryk, E., Bagley, K. A., Thibodeau, D. L., Bauscher, M., Mäntele, W., and Breton, J. (1990) *FEBS Lett. 266*, 59−62.
7. Stowell, M. H. B., McPhillips, T. M., Rees, D. C., Solitis, S. M., Abresch, E., and Feher, E. (1997) *Science 276*, 812−816.
8. Graige, M. S., Feher, G., and Okamura, M. Y. (1998) *Proc. Natl. Acad. Sci. U.S.A. 95*, 11679−11684.
9. Rabenstein, B., Ullmann, G. M., and Knapp, E. W. (2000) *Biochemistry 39*, 10487−10496.
10. Alexov, E. G., and Gunner, M. R. (1999) *Biochemistry 38*, 8253−8270.
11. Ermler, U., Fritzsch, G., Buchanan, S. K., and Michel, H. (1994) *Structure 2*, 925−936.
12. Okamura, M. Y., and Feher, G. (1995) in *Anoxygenic Photosynthetic Bacteria* (Blankenship, R. E., Madigan, M. T., and Bauer, C. E., Eds.) pp 577−594, Kluwer Academic Publishers, Dordrecht, The Netherlands.
13. Takahashi, E., and Wraight, C. A. (1994) in *Advances in Molecular and Cell Biology: Molecular Processes in Photosynthesis* (Barber, J., Ed.) pp 197−251, JAI Press, Greenwich.
14. Nabedryk, E., Breton, J., Hienerwadel, R., Fogel, C., Mäntele, W., Paddock, M. L., and Okamura, M. Y. (1995) *Biochemistry 34*, 14722−12732.
15. Hinerwadel, R., Grzybek, S., Fogel, C., Kreutz, W., Okamura, M. Y., Paddock, M. L., Breton, J., Nabedryk, E., and Mäntele, W. (1995) *Biochemistry 34*, 2832−2843.
16. Nabedryk, E., Breton, J., Okamura, M. Y., and Paddock, M., L. (1998) *Biochemistry 37*, 14457−14462.
17. Grafton, A. K., and Wheeler, R. A. (1999) *J. Phys. Chem. B 103*, 5380−5387.
18. Takahashi, E., and Wraight, C. A. (1990) *Biochim. Biophys. Acta 1020*, 107−111.
19. Takahashi, E., and Wraight, C. A. (1992) *Biochemistry 31*, 855−866.
20. Paddock, M. L., Rongey, S. H., McPherson, P. H., Juth, A., Feher, G., and Okamura, M. Y. (1994) *Biochemistry 33*, 734−745.
21. Brooks, B. R., Bruccoleri, R. E., Olafson, B. D., States, D. J., Swaminathan, S., and Karplus, M. (1983) *J. Comput. Chem. 4*, 187−217.
22. Gibas, C. J., and Subramaniam, S. (1996) *Biophys. J. 71*, 138−147.
23. Ullmann, G. M., Muegge, I., and Knapp, E. W. (1996) in *The Reaction Centers of Photosynthetic Bacteria: Structure and Dynamics* (Michel-Beyerle, E. M., Ed.) pp 143−155, Springer, Berlin.
24. Rabenstein, B., and Knapp, E. W. (2001) *Biophys. J. 80*, 1141−1150.
25. Popovic, D. M., Zaric, S. D., Rabenstein, B., and Knapp, E. W. (2001) *J. Am. Chem. Soc. 123*, 6040−6053.
26. Rabenstein, B., Ullmann, G. M. and Knapp, E. W. (1998) *Biochemistry 37*, 2488−2495.
27. Popovic, D. M., Zmiric, A., Zaric, S. D., and Knapp, E. W. (2002) *J. Am. Chem. Soc. 124*, 3775−3782.
28. MacKerell, A. D. J., Bashford, D., Bellott, M., Dunbrack, R. L., Jr., Evanseck, J. D., Field, M. J., Fischer, S., Gao, J., Guo, H., Ha, S., Joseph-McCarthy, D., Kuchnir, L., Kuczera, K., Lau, F. T. K., Mattos, C., Michnick, S., Ngo, T., Nguyen, D. T., Prodhom, B., Reiher, W. E., III, Roux, B., Schlenkrich, M., Smith, J. C., Stote, R., Straub, J., Watanabe, M., Wiórkiewicz-Kuczera, J., Yin, D., and Karplus, M. (1998) *J. Phys. Chem. B 102*, 3586−3616.

29. Bashford, D., and Karplus, M. (1990) *Biochemistry 29*, 10219−10225.
30. Rabenstein, B. (1999) *Karlsberg online manual*, http://lie.chemie.fu-berlin.de/karlsberg/.
31. Rabenstein, B., Ullmann, G. M., and Knapp, E. W. (1998) *Eur. Biophys. J. 27*, 626−637.
32. Honig, B., and Nicholls, A. (1995) *Science 268*, 1144−1149.
33. Warshel, A., and Russel, S. T. (1984) *Q. Rev. Biophys. 17*, 283−422.
34. Warshel, A., and Åqvist. (1991) *Annu. Rev. Biophys. Biophys. Chem. 20*, 267−298.
35. Warshel, A., Papazyan, A., and Muegge, I. (1997) *J. Biol. Inorg. Chem. 2*, 143−152.
36. Rabenstein, B., and Knapp, E. W. (2003) in *Bioenergetics* (Wheeler, R. A., Ed.) American Chemical Society, Washington, DC, in press.
37. Wraight, C. A. (1998) in *Photosynthesis: Mechanisms and Effects, Vol. 2* (Garab, G., Ed.) pp 693−698, Kluwer Academic Publishers, Dordrecht, The Netherlands.
38. Swallow, A. J. (1982) in *Function of Quinones in Energy Conserving Systems* (Trumpower, B. L., Ed.) pp 59−72, Academic Press, New York.
39. Prince, R. C., Dutton, P. L. and Bruce, J. M. (1983) *FEBS Lett. 160*, 273−276.
40. Prince, R. C., and Dutton, P. L. (1978) in *The Photosynthetic Bacteria* (Clayton, R. K., and Sistrom, W. R., Eds.) pp 439−453, Plenum Press, New York.
41. Reed, D. W., Zankel, K. L., and Clayton, R. K. (1969) *Proc. Natl. Acad. Sci. U.S.A. 63*, 42−46.
42. Dutton, P. L., Leigh, J. S., and Wraight, C. A. (1973) *FEBS Lett. 36*, 169−173.
43. Arata, H., and Nishimura, M. (1983) *Biochim. Biophys. Acta 726*, 394−401.
44. Prince, R. C., and Dutton, P. L. (1976) *Arch. Biochem. Biophys. 172*, 329−334.
45. Maróti, P., and Wraight, C. W. (1988) *Biochim. Biophys. Acta 934*, 329−347.
46. Turzó, K., Laczkó, G., Filus, Z., and Maróti, P. (2000) *Biophys. J. 79*, 14−25.
47. Mancino, L. J., Dean, D. P., and Blankenship, R. E. (1984) *Biochim. Biophys. Acta 764*, 46−54.
48. Kleinfeld, D., Okamura, M. Y., and Feher, G. (1984) *Biochim. Biophys. Acta 766*, 126−140.
49. Tandori, J., Sebban, P., Michel, H., and Baciou, L. (1999) *Biochemistry 38*, 13179−13187.
50. Prince, R. C., and Dutton, P. L. (1978) *Arch. Biochem. Biophys. 172*, 329−334.
51. Kálmán, L., and Maróti, P. (1997) *Biochemistry 36*, 15269−15276.
52. Takahashi, E., Wells, T. A., and Wraight, C. A. (2001) *Biochemistry 40*, 1020−1028.
53. O'Malley, P. J. (1999) *Biochim. Biophys. Acta 1411*, 101−113.
54. Brzezinski, P., Paddock, M. L., Okamura, M. Y., and Feher, G. (1997) *Biochim. Biophys. Acta 1321*, 149−156.
55. Nabedryk, E., Breton, J., Okamura, M. Y., and Paddock, M. L. (2001) *Biochemistry 40*, 13826−13832.
56. Tandori, J., Baciou, L., Alexov, E., Maróti, P., Schiffer, M., Hanson, D. K., and Sebban, P. (2001) *J. Biol. Chem. 276*, 45513−45515.
57. Miksovska, J., Maróti, P., Tandori, J., Schiffer, M., Hanson, D. K., and Sebban, P. (1996) *Biochemistry 35*, 15411−15417.
58. Miksovska, J., Schiffer, M., Hanson, D. K., and Sebban, P. (1999) *Proc. Natl. Acad. Sci. U.S.A. 96*, 14348−14353.
59. Maróti, P., Hanson, D. K., Schiffer, M., and Sebban, P. (1995) *Nat. Struct. Biol. 2*, 1057−1059.
60. Miksovska, J., Maróti, P., Schiffer, M., Hanson, D. K., and Sebban, P. (1995) in *Photosynthesis: From Light to Biospher* (Mathis, P., Ed.) pp 467−470, Kluwer Academic Publishers, Dordrecht, The Netherlands.
61. Ädelroth, P., Paddock, M. L., Sagle, L. B., Feher, G., and Okamura, M. Y. (2000) *Proc. Natl. Acad. Sci. U.S.A. 97*, 13086−13091.
62. Knapp, E. W., and Nilsson, L. (1990) in *Proceedings of the 23rd Jerusalem Symposia on Quantum Chemistry and Biochemistry, Vol. 23* (Jortner, J., and Pullman, B., Eds.) pp 389−412, Reidel, Amsterdam.
63. Hanson, D. K., Baciou, L., Tiede, D. M., Nance, S. L., Schiffer, M., and Sebban, P. (1992) *Biochim. Biophys. Acta 1102*, 260−265.
64. Pokkuluri, P. R., Laible, P. D., Deng, Y.-L., Wong, T. N., Hanson, D. K., and Schiffer, M. (2002) *Biochemistry 41*, 5998−6007.
65. Maróti, P., Hanson, D. K., Baciou, L., Schiffer, M. and Sebban, P. (1994) *Proc. Natl. Acad. Sci. U.S.A. 91*, 5617−5621.
66. Abresch, E. C., Paddock, M. L., Stowell, M. H. B., McPhillips, T. M., Axelrod, H. L., Soltis, S. M., Rees, D. C., Okamura, M. Y., and Feher, G. (1998) *Photosynth. Res. 55*, 119−125.
67. Rongey, S. H., Juth, A. L., Paddock, M. L., Feher, G., and Okamura, M. Y. (1995) *Biophys. J. 68*, A247.
68. Takahashi, E., and Wraight, C. A. (1995) *Biophys. J. 68*, A95.
69. Takahashi, E., and Wraight, C. A. (1996) *Proc. Natl. Acad. Sci. U.S.A. 93*, 2640−2645.
70. Takahashi, E., and Wraight, C. A. (1998) *Biophys. J. 74*, A76.
71. Paddock, M. L., McPherson, P. H., Feher, G., and Okamura, M. Y. (1990) *Proc. Natl. Acad. Sci. U.S.A. 87*, 6803−6807.
72. Paddock, M. L., Adelroth, P., Chang, C., Abresch, E. C., Feher, G., and Okamura, M. Y. (2001) *Biochemistry 40*, 6893−6902.
73. Paddock, M. L., Feher, G., and Okamura, M. Y. (2000) *Proc. Natl. Acad. Sci. U.S.A. 97*, 14457−14462.
74. Ädelroth, P., Paddock, M. L., Tehrani, A., Beatty, J. T., Feher, G., and Okamura, M. Y. (2001) *Biochemistry 40*, 14538−14546.

BI026781T